Robust Single Molecule Magnet Monolayers on Graphene and Graphite with Magnetic Hysteresis up to 28 K

Lukas Spree,* Fupin Liu, Volker Neu, Marco Rosenkranz, Georgios Velkos, Yaofeng Wang, Sandra Schiemenz, Jan Dreiser, Pierluigi Gargiani, Manuel Valvidares, Chia-Hsiang Chen, Bernd Büchner, Stanislav M. Avdoshenko,* and Alexey A. Popov*

The chemical functionalization of fullerene single molecule magnet $Tb_2@C_{80}(CH_2Ph)$ enables the facile preparation of robust monolayers on graphene and highly oriented pyrolytic graphite from solution without impairing their magnetic properties. Monolayers of endohedral fullerene functionalized with pyrene exhibit magnetic bistability up to a temperature of 28 K. The use of pyrene terminated linker molecules opens the way to devise integration of spin carrying units encapsulated by fullerene cages on graphitic substrates, be it single-molecule magnets or qubit candidates.

1. Introduction

The realization of single-spin devices for magnetic memory or quantum information processing relies on the possibility to create arrays of discrete magnetic units on suitable substrates, which can function as device electrodes. Useful properties of these units, such as the magnetic bistability and the long life-time of magnetic states, should be sustained on contact. On a more practical side, the magnetic units should possess a certain thermal and chemical stability to facilitate their processing. Concepts of several devices based on single-molecule magnets (SMMs) were already successfully realized,[1] but at this moment their function has only been demonstrated at sub-Kelvin temperatures. In the meantime, continuous development of lanthanide SMMs boosted their temperature range up to 80 K,[2] but the transfer of these properties from the bulk to nanoscale assemblies is lagging behind, and the magnetic bistability of SMM submonolayers is limited to 10 K at this moment.[3]

Here, we describe a breakthrough in the field of surface-supported SMMs through the use of chemically functionalized magnetic metallofullerenes. We show that the functionalization of $Tb_2@C_{80}(CH_2Ph)$ with a pyrene-terminated linker molecule facilitates the formation of self-assembled monolayers (SAMs) on substrates like graphene and highly oriented pyrolytic graphite (HOPG). Layers of these molecules exhibit magnetic hysteresis up to 28 K, showing no negative impact of the functionalization or deposition process on the magnetic properties. The exceptionally simple method of obtaining 2D-fullerene-graphene hybrid materials described here opens the way for device integration of spin-carrying endohedral fullerenes, be it SMMs or qubit candidates.

$Tb_2@C_{80}(CH_2Ph)$ ({Tb$_2$} hereafter) is a member of the lanthanide dimetallofullerene series with unconventional electronic structure and excellent SMM performance.[4] The endohedral metal dimer in {Tb$_2$} features a single-electron covalent Tb—Tb bond and can be formally described as a [Tb^{3+}–e–Tb^{3+}] unit. This bond is responsible for the unique magnetic structure of the molecule. Two Tb ions have moderately large uniaxial magnetic anisotropy with a collinear arrangement of their magnetic moments. Each of the local Tb-4f moments is coupled ferromagnetically to the spin of the unpaired electron residing on the Tb—Tb bonding molecular orbital with spd-hybrid character. As a result, {Tb$_2$} has a large magnetic moment of 19 μ_B and demonstrates SMM behavior with a high blocking temperature of 29 K surpassed only by some metallocene-based SMMs.[2,5] Besides, {Tb$_2$} shows exceptionally broad magnetic hysteresis with a coercive field of 8 Tesla at 10 K. Despite the unconventional lanthanide oxidation state of +2.5, {Tb$_2$} is an air-stable compound and does not require special handling conditions. This combination of outstanding SMM properties and

L. Spree, F. Liu, M. Rosenkranz, G. Velkos, Y. Wang, S. Schiemenz,
C.-H. Chen, B. Büchner, S. M. Avdoshenko, A. A. Popov
Institute for Solid State Research
Leibniz Institute for Solid State and Materials Research
Helmholtzstraße 20, 01069 Dresden, Germany
E-mail: l.spree@ifw-dresden.de; s.avdoshenko@ifw-dresden.de;
a.popov@ifw-dresden.de
V. Neu
Institute for Integrative Nanosciences
Leibniz Institute for Solid State and Materials Research
Helmholtzstraße 20, 01069 Dresden, Germany
J. Dreiser
Swiss Light Source
Paul Scherrer Institute
Villigen PSI CH-5232, Switzerland
P. Gargiani, M. Valvidares
ALBA Synchrotron Light Source
Barcelona E-08290, Spain
C.-H. Chen
Department of Medicinal and Applied Chemistry
Kaohsiung Medical University
Kaohsiung 807, Taiwan

**ADVANCED
SCIENCE NEWS**

www.advancedsciencenews.com

**ADVANCED
FUNCTIONAL
MATERIALS**

www.afm-journal.de

stability makes {Tb$_2$} a prime candidate for the seamless integration into spintronic devices.

2. Results and Discussion

2.1. Fullerene Derivatization

The benzyl group on {Tb$_2$}, which is needed for stabilization of the otherwise open-shell electronic structure, precludes the clean evaporation of the molecule onto surfaces. A straightforward way to overcome this limitation and facilitate the formation of SAMs is the functionalization of the fullerene with a linker moiety, terminated by a functional group tailored to the desired substrate. Here, we concentrated on the deposition of {Tb$_2$} onto graphene and graphite (HOPG). Pyrene, known to show high affinity to graphitic substrates, was used to functionalize SMMs for their deposition on graphene and nanotubes in the past.[1b,6] To introduce pyrene groups to {Tb$_2$}, we utilized the approach developed by Zaragoza-Galán et al.[7] for functionalization of C$_{60}$ with pyrene groups and then used the derivative for subsequent SAM growth. In short, 3,5-bis(4-(pyren-1-yl)butoxy) benzaldehyde was synthesized and then reacted with {Tb$_2$} and *N*-methylglycine (sarcosine) in o-dichlorobenzene at 140 °C (**Figure 1**a). The crude product of this dipolar cycloaddition reaction contained the targeted fulleropyrrolidine monoadduct bearing two pyrene groups, {Tb$_2$}-pyr$_2$, along with unreacted educts and several other fulleropyrrolidine adducts. The chromatographic isolation and characterization
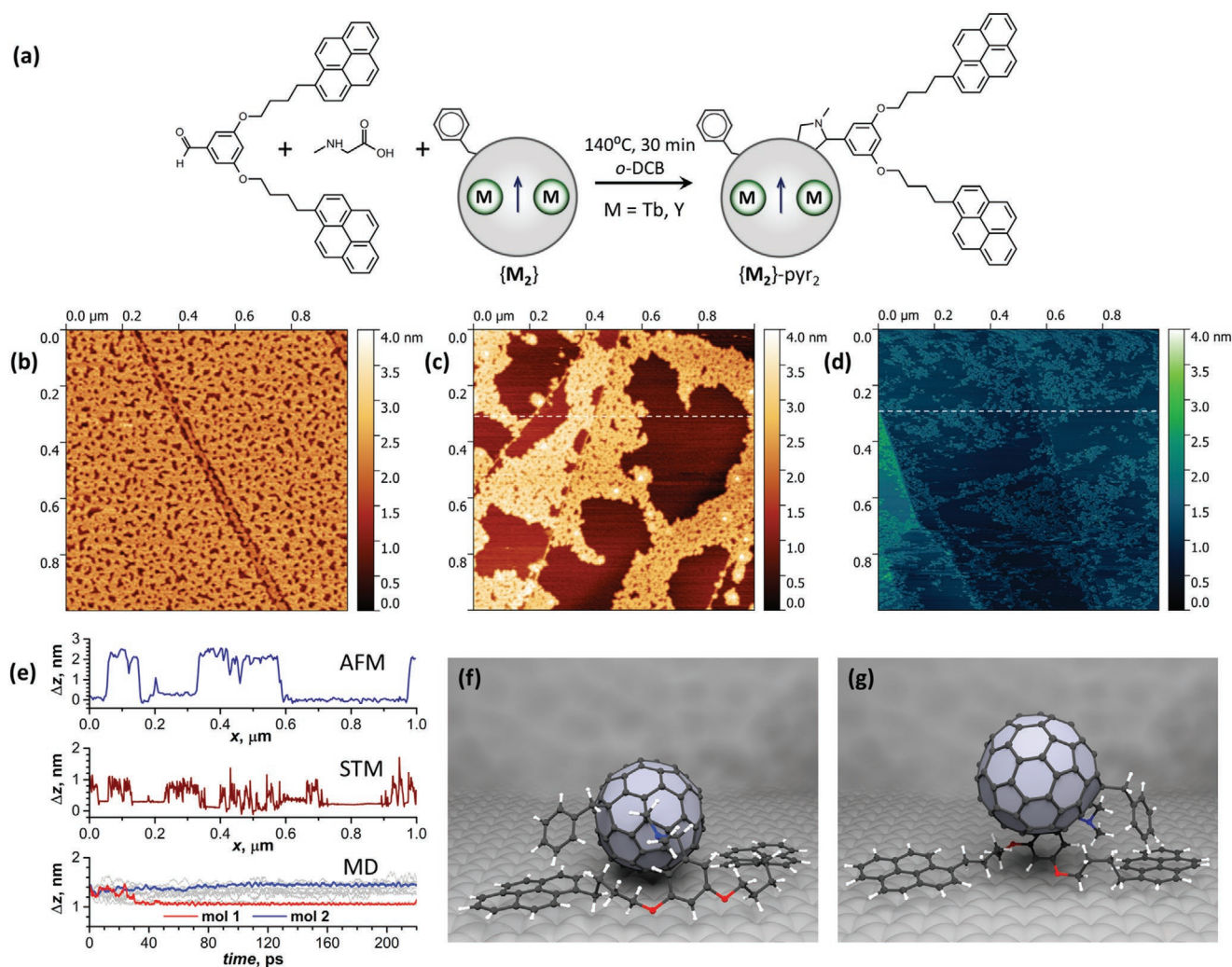

Figure 1. a) Functionalization of {M$_2$} (M = Tb, Y) with pyrene anchor groups via dipolar cycloaddition reaction giving {M$_2$}-pyr$_2$; the arrow between metal atoms indicates unpaired electrons residing on the M—M bonding orbital. b,c) AFM topography of freshly prepared {Tb$_2$}-pyr$_2$ (sub)monolayer films on HOPG grown from DMF (b) and toluene (c) (room temperature, peak force tapping mode at 150 pN). d) STM topography of {Tb$_2$}-pyr$_2$ submonolayer on HOPG grown from toluene after 24 h degassing in UHV conditions (room temperature, bias 1.7 V, current 150 pA). e) Height profiles along the dashed lines in (c, AFM) and (d, STM) and the height profiles for a stripe of 12-molecules from molecular dynamics simulations (MD). f,g) Laying-down and standing-up configurations of {Tb$_2$}-pyr$_2$ molecule on graphene from MD simulations, corresponding to mol 1 and mol 2 profiles in (e) at the time moment 120 ps.

of {Tb$_2$}-pyr$_2$ are shown in the Supporting Information. The analogous reaction was also performed with Y$_2$@C$_{80}$(CH$_2$Ph) ({Y$_2$}) to obtain {Y$_2$}-pyr$_2$.

2.2. Self-Assembled Monolayers

{Tb$_2$}-pyr$_2$ is soluble in toluene and, to a lesser extent, dimethylformamide (DMF). Solutions of {Tb$_2$}-pyr$_2$ in these solvents were used for self-assembly of the fullerene derivative on two types of graphitic substrates, freshly cleaved HOPG and chemical vapor deposition graphene on SiO$_2$/Si. The binding of {Tb$_2$}-pyr$_2$ to either substrate is very easily achieved by depositing a droplet of the solution for some time, before washing said droplet and excess fullerene molecules from the substrate with clean solvent. In the case of DMF, a drop of ≈3 mm diameter is stable for at least 30 min under a glass lid. Toluene is more volatile and tends to evaporate in under 10 min, leaving precipitated fullerene molecules on the substrate, which can be washed off with clean toluene. The whole procedure is described in full detail in the Supporting Information. Atomically flat graphene layers in HOPG substrate give a clear contrast with the fullerene islands and thus allow detailed analysis of the layer coverage and thickness. Thus, in the discussion

below we focus on {Tb$_2$}-pyr$_2$ SAMs grown on HOPG. Characterization of the films grown on graphene/SiO$_2$/Si by atomic force microscopy (AFM) and Raman spectroscopy is provided in the Supporting Information.

Characterization of the resulting {Tb$_2$}-pyr$_2$ films on HOPG by atomic force microscopy (AFM) reveals, that the deposition from DMF leads to the formation of a layer with uniform thickness in the whole area exposed to the solution (Figure 1b, see also Figure S16a, Supporting Information, for different magnification). The layer has orifices with the lateral size of 20–40 nm, and the height profile measurements along these orifices gives the layer thickness in the order of 1.8–2 nm (Figure S16b, Supporting Information), indicating that the layer has a single-molecule thickness. Excluding the area of the orifices allows estimation of the surface coverage in DMF-deposited fullerene layer as 80–85%.

The deposition from toluene solution leads to the formation of smaller islands with gaps of clean substrate in between (**Figure 2**c and Figure S17a, Supporting Information). This is likely owed to the difference in solubility, favoring the binding to the substrate in case of DMF and the removal of some of the deposited {Tb$_2$}-pyr$_2$ when rinsing with toluene. The coverage of the substrate with fullerene estimated from AFM topographies is about 35% (Figure S17b, Supporting Information).
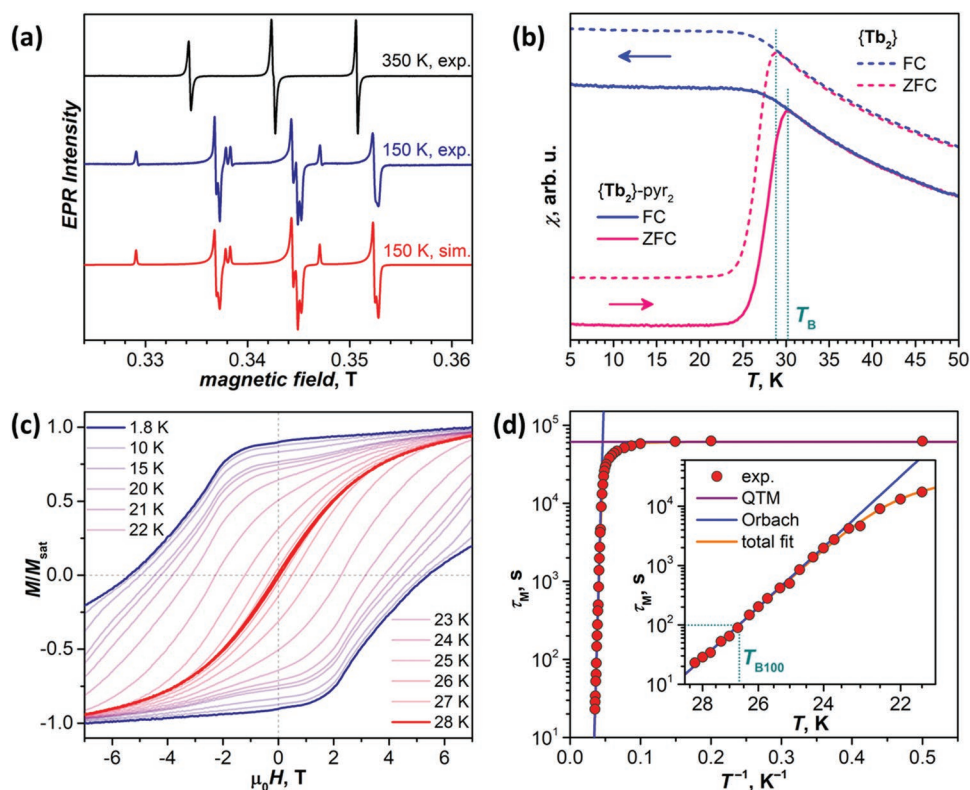

Figure 2. a) EPR spectra of {Y$_2$}-pyr$_2$ in toluene at 350 K (g_{iso} = 1.9733, a_{iso}(^{89}Y) = 222 and 230 MHz) and at 150 K compared to the simulated spectrum for 150 K. b) Magnetic susceptibility of {Tb$_2$}-pyr$_2$ (solid lines) and {Tb$_2$} (dashed lines) measured during warming up of zero-field cooled sample (ZFC) and during cooling down in magnetic field (FC); magnetic field 0.2 T, temperature sweep rate 5 K min^{-1}, the curves for two compounds are shown with a vertical off-set, vertical dotted lines mark blocking temperature of magnetization T_B. c) Magnetic hysteresis curves of {Tb$_2$}-pyr$_2$ measured between 1.8 and 28 K; magnetic field sweep rate 2.9 mT s^{-1}. d) Magnetization relaxation times of {Tb$_2$}-pyr$_2$ determined at different temperatures; straight lines are contributions of the QTM and Orbach relaxation mechanisms, the orange curve is a total fit including QTM, Raman, and Orbach processes: $\tau_M^{-1} = \tau_{QTM}^{-1} + C_{Ram}T^n + \tau_0^{-1}\exp(-U^{eff}/T)$. The inset magnifies the temperature range 21–29 K and shows the definition of 100-s blocking temperature T_{B100}.

The characterization of $\{Tb_2\}$-pyr_2 deposited on HOPG from a toluene solution by scanning tunneling microscopy (STM) yields similar topography to the AFM technique with the coverage near 30% (Figure 1d). The measurement was complicated by the tendency of deposited molecules to attach to the STM tip, and the image in Figure 1d was acquired by keeping the tip relatively far away from the sample. The possibility to perform both AFM and STM topographic characterization at room temperature indicates that the molecules are anchored to the substrate even if the layer is not closely packed.

The well-defined borders between fullerene islands and bare substrate in toluene-grown SAMs are instrumental for a more reliable determination of the film thickness than for the SAM deposited from DMF. The height profiles of $\{Tb_2\}$-pyr_2 films extracted from Figures 1b (AFM) and 1c (STM) prove the formation of layers with uniform height (Figure 1d). However, noticeable distinction of height differences between unfunctionalized graphite and the fullerene islands were detected by AFM (2 nm) and STM (0.8 nm). Molecular dynamics (MD) simulations showed that a single $\{Tb_2\}$-pyr_2 molecule on graphene would adopt a laying-down conformation with the apparent height of 1.1 nm, corresponding to the size of the fullerene cage (Figure 1e). However, when surrounded by other molecules, either of solvent (Supporting Information) or of $\{Tb_2\}$-pyr_2 neighbors, the fullerene core tends to elevate above the substrate, giving the height of 1.5–1.6 nm for a still rather sparse arrangement of molecules in the island (Figure 1f, see Supporting Information for more details on molecular dynamics simulations). Further increase of the molecular height may naturally occur in a densely packed layer. Similar conclusions were obtained in the study of functionalized C_{60} SAMs on graphene.[8] We thus conclude that the results of AFM and STM measurements point to the single-molecule thickness of the $\{Tb_2\}$-pyr_2 SAMs, and that the apparent height difference between the two techniques can likely be attributed to the different sample-tip interactions of the two methods. In particular, different local density of states in graphite and fullerene can strongly affect the tunneling current, giving different apparent layer heights depending on bias and current settings.

2.3. Magnetic Properties of $\{M_2\}$-pyr_2

Facile preparation of SAMs indicates that they might be well suited for design of molecular spintronic devices based on integration with graphene electronics, unless magnetic properties of $\{Tb_2\}$ are negatively affected by derivatization and deposition. To evaluate the effect of derivatization, we characterized spin properties of $\{Y_2\}$-pyr_2 and $\{Tb_2\}$-pyr_2 by electron paramagnetic resonance (EPR) spectroscopy and SQUID magnetometry, respectively.

$\{Y_2\}$ exhibits a very characteristic hyperfine structure in its EPR spectrum caused by the interaction of the unpaired electron spin residing on the Y—Y bonding orbital with nuclear spins of ^{89}Y ($I_Y = 1/2$). The isotropic hyperfine coupling constant in $\{Y_2\}$ is $a_{iso}(^{89}Y) = 224$ MHz and the g-factor is 1.9733.[4c] $\{Y_2\}$-pyr_2 has a similar hyperfine structure in toluene solution (Figure 2a), but the rotational averaging appears incomplete even at 350 K, leading to a distorted intensity ratio (see

Supporting Information for further analysis). The measurement in frozen solution at 150 K revealed a well-resolved powder-like pattern with slightly distorted axial g-tensor (1.9591, 1.9616, and 1.9997) and two inequivalent Y atoms with axial $A(^{89}Y)$-tensors and principal $A_z/A_{x,y}$ values of 246/219 and 258/207 MHz (see further discussion in Supporting Information). Two Y atoms in $\{Y_2\}$-pyr_2 remain inequivalent at 350 K. Thus, EPR measurements prove that the cycloaddition leaves the single-electron M—M bond intact and hinders rotation of the M_2 dimer inside a fullerene cage.

The effect of the cycloaddition on the SMM behavior of the endohedral $[Tb^{3+}$–e–$Tb^{3+}]$ unit was studied by SQUID magnetometry of a powder $\{Tb_2\}$-pyr_2 sample. Blocking of magnetization, as determined from the comparison of a field-cooled and a zero-field-cooled temperature sweep (5 K min^{-1}) is observed at 30.3 K (Figure 2b), which is 1.4 K higher than in the pristine $\{Tb_2\}$.[4a] Another SMM figure of merit, the 100-s blocking temperature T_{B100}, is found to be 26.6 K in $\{Tb_2\}$-pyr_2 versus 25.2 K in $\{Tb_2\}$. When measured with a moderate sweep rate of 2.9 mT s^{-1}, magnetic hysteresis in $\{Tb_2\}$-pyr_2 is still open at 28 K (Figure 2c). The hysteresis of $\{Tb_2\}$-pyr_2 is narrower than in $\{Tb_2\}$, but still exhibits a very large coercive field of 5.0–5.4 T below 20 K.

To elucidate the relaxation mechanism, magnetization relaxation times were measured at different temperatures between 2 and 28 K by magnetizing the sample at 7 T, quickly removing the external field and measuring the magnetization decay of the sample. The decay curves and their fitting with a stretched exponential function are presented in Supporting Information. Figure 2d plots the obtained relaxation times as a function of reciprocal temperature. In zero magnetic field, $\{Tb_2\}$-pyr_2 shows two distinct relaxation regimes. Below 10 K, the relaxation time of 17.1(3) h is temperature-independent, which is a characteristic sign of the quantum tunneling of magnetization (QTM). Above 22 K, the relaxation is dominated by the Orbach mechanism as evidenced by the Arrhenius behavior, $\tau_M^{-1} = \tau_0^{-1} \exp(-U^{eff}/T)$, with the effective barrier U^{eff} of 725(6) K and τ_0 of 1.6(4) 10^{-10} s. For comparison, the pristine $\{Tb_2\}$ exhibits the QTM mechanism with τ_{QTM} of 18.0(3) h below 15 K and thermally activated relaxation with the barrier of 799(2) K above 20 K.[4a] Cycloaddition thus reduced the U^{eff} barrier by 10%. The thermal barrier U^{eff} corresponds to the exchange excitation, when one Tb magnetic moment attains opposite orientation versus the magnetic moment of the other Tb ion, which remains ferromagnetically coupled to the unpaired electron spin. The somewhat smaller U^{eff} value obtained for $\{Tb_2\}$-pyr_2 when compared to $\{Tb_2\}$ shows that the exchange interactions within the Tb_2 dimer are affected when the fullerene π-system is changed in the course of exohedral derivatization, but the effect is not very pronounced and the overall properties of the magnetic core remain similar. Evidently, the chemical functionalization even improves some SMM parameters, as it was found in another fullerene-SMM, $DySc_2N@C_{80}$.[9]

2.4. Surface Magnetism of $\{Tb_2\}$-pyr_2 Monolayers

Surface magnetism of $\{Tb_2\}$-pyr_2 monolayers on HOPG and graphene was studied by X-ray magnetic circular dichroism
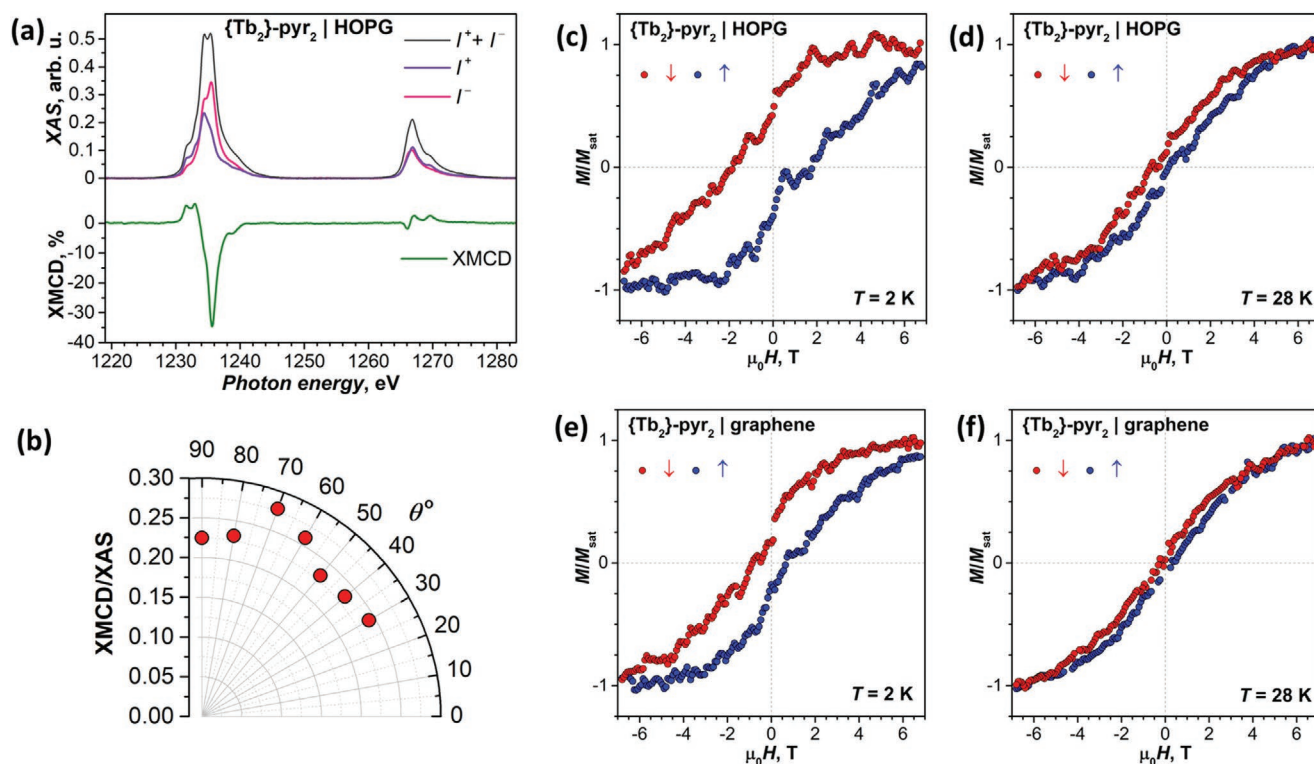
Figure 3. a) Circularly polarized X-ray absorption spectra of {Tb$_2$}-pyr$_2$ monolayer on HOPG: I^+ and I^- are clockwise and counter-clockwise circular polarizations, their sum gives non-polarized spectrum, whereas their difference is XMCD; $T = 30$ K, $\mu_0H = 6$ T, normal X-ray incidence. b) Angular dependence of the XMCD on HOPG, $T = 2$ K, θ is the angle between X-ray beam and the surface (90° corresponds to the normal incidence). c,d) Magnetic hysteresis curves of {Tb$_2$}-pyr$_2$ monolayer on HOPG measured by XMCD at 2 and 28 K. e,f) Magnetic hysteresis curves of {Tb$_2$}-pyr$_2$ monolayer on graphene measured by XMCD at 2 and 28 K (see Figure S30, Supporting Information, for measurements at other temperatures). Normal X-ray and magnetic field incidence, sweep rate 1.5 T min^{-1}.

(XMCD) with synchrotron radiation at the Swiss Light Source, Paul Scherrer Institute (X-Treme beamline[10]) and ALBA (Boreas beamline[11]). In agreement with the AFM and STM results discussed above, the ratio of X-ray absorption intensity at the Tb-$M_{4,5}$ edge for the {Tb$_2$}-pyr$_2$ SAMs deposited from DMF and toluene is close to 2:1 (Figure S29, Supporting Information), proving that the SAMs deposited from DMF do not exceed a monolayer coverage. Since SAMs deposited from and rinsed with DMF showed higher and more uniform coverage of the substrate (Figure 1b,c), we discuss XMCD measurements performed for such monolayers here. Results obtained for toluene-deposited SAMs are, however, similar (see Supporting Information).

X-ray absorption spectra of a {Tb$_2$}-pyr$_2$ monolayer at the Tb-$M_{4,5}$ edge measured with clockwise and counter-clockwise polarizations of incoming X-ray beam develop a dichroism in the presence of a net magnetization along the beam direction (**Figure 3**a). A magnetic field collinear with the X-ray beam was employed in the measurements, and therefore the size of the XMCD signal is proportional to the magnetization in the direction of the X-ray beam. The angular dependence of the XMCD was investigated by varying the incidence angle of the magnetic field and X-ray beam with respect to the sample surface. The lack of a strong angular dependence as seen in Figure 3b shows that Tb$_2$ dimers attain different orientations in the {Tb$_2$}-pyr$_2$

monolayer on HOPG with a slight preference for the 70° orientation versus the substrate.

The maximum of the XMCD signal at 1235 eV was used to monitor the changes of the SAM magnetization during magnetic field sweeps. At 2 K, {Tb$_2$}-pyr$_2$ monolayers exhibit open magnetic hysteresis on both HOPG and graphene substrates (Figure 3c,e). Measurements with different X-ray fluxes revealed that the increase of the X-ray intensity leads to a narrowing of the hysteresis (Figure S32, Supporting Information), which indicates that the hysteresis width is limited by the demagnetization effect of the X-rays.[3f,12] Thus, the intrinsic hysteresis of the {Tb$_2$}-pyr$_2$ monolayer is probably broader, in line with the bulk magnetization measurement (Figure 2c). Interestingly, on graphene the hysteresis opening is narrower than on HOPG, which may indicate that the electronic properties of the substrate influence the relaxation of magnetization,[6d] although the charging of the silicon substrate may have a similar effect and thus cannot be excluded either. Spectacularly, the hysteresis of {Tb$_2$}-pyr$_2$ monolayers remains open up to 28 K and is closed at 30 K (Figure 3d,f and Figure S31, Supporting Information, for intermediate temperatures and 30 K). Thus, {Tb$_2$}-pyr$_2$ retains slow relaxation of magnetization in monolayer form on conducting graphitic substrates and exhibits measurable magnetic bistability in the same temperature range as in the bulk powder form.

**ADVANCED
SCIENCE NEWS**

www.advancedsciencenews.com

**ADVANCED
FUNCTIONAL
MATERIALS**

www.afm-journal.de

3. Conclusions

Over a decade after the first observation of magnetic hysteresis in an Fe_4 monolayer,[13] the temperature range in which this phenomenon could be observed for SMM monolayers expanded from sub-K regime to 10 K.[3b,c,f] With this robust fullerene-based SMM, we make a major step forward and push the temperature range of the phenomenon to 28 K. This is comparable to Ho atoms on a thin layer of MgO|Ag(100), which demonstrate broad magnetic hysteresis up to 30 K[14] and magnetic bistability up to 45 K.[15] But atomic submonolayers are stable only in UHV condition and require cryogenic temperature deposition to avoid cluster formation and to maintain a stable adsorption site on the surface since Ho atoms start to move on the surface already at 50 K. The solution-based preparation procedure of the $\{Tb_2\}$-pyr$_2$ SAMs on graphitic substrates is exceptionally simple and fast, consumes tiny amounts of material, can be carried out in air, and does not require UHV conditions or special temperature regimes. The method should lend itself well to larger scale manufacturing techniques, like ink-jet printing and the use of nanospotters, and is compatible with graphene electronics and spintronics,[16] opening the way toward patterned devices with hybrid graphene-SMM interfaces. Furthermore, while $\{Tb_2\}$ is an excellent SMM, its non-4f analogs $\{Y_2\}$ and especially $\{Sc_2\}$ have recently been shown to be promising qubit candidates,[17] and the functionalization and deposition methods presented here might be a way of addressing them on a single molecule level. Finally, the linker molecule presented in this work is but the first option tested, and other approaches to hybrids of fullerenes with graphene and 2D materials can be applied to create assemblies with required properties.[18] For instance, increasing the number of surface binding pyrene groups in the linker molecule has been shown to enhance the stability of the resulting SAMs,[19] and examples with fullerenes can already be found in literature.[8]

Supporting Information

Supporting Information is available from the Wiley Online Library or from the author.

Acknowledgements

Conflict of Interest

The authors declare no conflict of interest.

Author Contributions

L.S. synthesized $\{M_2\}$-pyr$_2$ derivatives with help from C.-H.C., performed their surface deposition, and led the whole project; F.L. synthesized $\{Tb_2\}$ and $\{Y_2\}$; V.N. and L.S. did AFM characterization; M.R. performed NMR and EPR measurements; L.S. and G.V. performed SQUID measurements; L.S., M.R., G.V., Y.W., and A.A.P. participated in XMCD measurements at SLS (together with J.D.) and at ALBA (together with P.G. and M.V.); L.S. and P.G. performed STM measurements at ALBA; S.S. did Raman mapping; S.M.A. performed computational modeling; A.A.P. conceived the project, analyzed EPR and XMCD data, and supervised all activities; L.S., S.M.A., and A.A.P. wrote the manuscript with contributions from all other co-authors.

Data Availability Statement

The data that support the findings of this study are available from the corresponding author upon reasonable request.

[1] a) R. Vincent, S. Klyatskaya, M. Ruben, W. Wernsdorfer, F. Balestro, *Nature* **2012**, *488*, 357; b) A. Candini, S. Klyatskaya, M. Ruben, W. Wernsdorfer, M. Affronte, *Nano Lett.* **2011**, *11*, 2634; c) M. Urdampilleta, S. Klyatskaya, J. P. Cleuziou, M. Ruben, W. Wernsdorfer, *Nat. Mater.* **2011**, *10*, 502; d) L. Bogani, W. Wernsdorfer, *Nat. Mater.* **2008**, *7*, 179.

[2] a) F.-S. Guo, B. M. Day, Y.-C. Chen, M.-L. Tong, A. Mansikkamäki, R. A. Layfield, *Science* **2018**, *362*, 1400; b) C. A. P. Goodwin, F. Ortu, D. Reta, N. F. Chilton, D. P. Mills, *Nature* **2017**, *548*, 439.

[3] a) M. Gonidec, R. Biagi, V. Corradini, F. Moro, V. De Renzi, U. del Pennino, D. Summa, L. Muccioli, C. Zannoni, D. B. Amabilino, J. Veciana, *J. Am. Chem. Soc.* **2011**, *133*, 6603; b) G. Serrano, E. Velez-Fort, I. Cimatti, B. Cortigiani, L. Malavolti, D. Betto, A. Ouerghi, N. B. Brookes, M. Mannini, R. Sessoli, *Nanoscale* **2018**, *10*, 2715; c) C.-H. Chen, L. Spree, E. Koutsouflakis, D. S. Krylov, F. Liu, A. Brandenburg, G. Velkos, S. Schimmel, S. M. Avdoshenko, A. Fedorov, E. Weschke, F. Choueikani, P. Ohresser, J. Dreiser, B. Büchner, A. A. Popov, *Adv. Sci.* **2021**, *8*, 2000777; d) A. Cornia, D. R. Talham, M. Affronte, in *Molecular Magnetic Materials*, (Eds: B. Sieklucka, D. Pinkowicz), Wiley-VCH, Weinheim **2017**, p. 187; e) M. Studniarek, C. Wäckerlin, A. Singha, R. Baltic, K. Diller, F. Donati, S. Rusponi, H. Brune, Y. Lan, S. Klyatskaya, M. Ruben, A. P. Seitsonen, J. Dreiser, *Adv. Sci.* **2019**, *6*, 1901736; f) C. Wäckerlin, F. Donati, A. Singha, R. Baltic, S. Rusponi, K. Diller, F. Patthey, M. Pivetta, Y. Lan, S. Klyatskaya, M. Ruben, H. Brune, J. Dreiser, *Adv. Mater.* **2016**, *28*, 5195.

[4] a) F. Liu, G. Velkos, D. S. Krylov, L. Spree, M. Zalibera, R. Ray, N. A. Samoylova, C.-H. Chen, M. Rosenkranz, S. Schiemenz, F. Ziegs, K. Nenkov, A. Kostanyan, T. Greber, A. U. B. Wolter, M. Richter, B. Büchner, S. M. Avdoshenko, A. A. Popov, *Nat. Commun.* **2019**, *10*, 571; b) F. Liu, L. Spree, D. S. Krylov, G. Velkos, S. M. Avdoshenko, A. A. Popov, *Acc. Chem. Res.* **2019**, *52*, 2981; c) F. Liu, D. S. Krylov, L. Spree, S. M. Avdoshenko, N. A. Samoylova,

2105516 (6 of 7)

M. Rosenkranz, A. Kostanyan, T. Greber, A. U. B. Wolter, B. Büchner, A. A. Popov, *Nat. Commun.* **2017**, *8*, 16098.

[5] a) K. R. McClain, C. A. Gould, K. Chakarawet, S. Teat, T. J. Groshens, J. R. Long, B. G. Harvey, *Chem. Sci.* **2018**, *9*, 8492; b) C. Gould, K. R. McClain, J. Yu, T. J. Groshens, F. Furche, B. G. Harvey, J. R. Long, *J. Am. Chem. Soc.* **2019**, *141*, 12967.

[6] a) S. Klyatskaya, J. R. G. Mascarós, L. Bogani, F. Hennrich, M. Kappes, W. Wernsdorfer, M. Ruben, *J. Am. Chem. Soc.* **2009**, *131*, 15143; b) L. Bogani, C. Danieli, E. Biavardi, N. Bendiab, A.-L. Barra, E. Dalcanale, W. Wernsdorfer, A. Cornia, *Angew. Chem., Int. Ed.* **2009**, *48*, 746; c) M. Lopes, A. Candini, M. Urdampilleta, A. Reserbat-Plantey, V. Bellini, S. Klyatskaya, L. Marty, M. Ruben, M. Affronte, W. Wernsdorfer, N. Bendiab, *ACS Nano* **2010**, *4*, 7531; d) C. Cervetti, A. Rettori, M. G. Pini, A. Cornia, A. Repollés, F. Luis, M. Dressel, S. Rauschenbach, K. Kern, M. Burghard, L. Bogani, *Nat. Mater.* **2015**, *15*, 164; e) Y. Zheng, L. Huang, Z. Zhang, J. Jiang, K. Wang, L.-M. Peng, G. Yu, *RSC Adv.* **2017**, *7*, 1776.

[7] G. Zaragoza-Galán, J. Ortíz-Palacios, B. X. Valderrama, A. A. Camacho-Dávila, D. Chávez-Flores, V. H. Ramos-Sánchez, E. Rivera, *Molecules* **2014**, *19*, 352.

[8] M. Garrido, J. Calbo, L. Rodríguez-Pérez, J. Aragó, E. Ortí, M. Á. Herranz, N. Martín, *Chem. Commun.* **2017**, *53*, 12402.

[9] a) C. H. Chen, D. S. Krylov, S. M. Avdoshenko, F. Liu, L. Spree, R. Westerström, C. Bulbucan, M. Studniarek, J. Dreiser, A. U. B. Wolter, B. Büchner, A. A. Popov, *Nanoscale* **2018**, *10*, 11287; b) Y. Li, T. Wang, H. Meng, C. Zhao, M. Nie, L. Jiang, C. Wang, *Dalton Trans.* **2016**, *45*, 19226.

[10] C. Piamonteze, U. Flechsig, S. Rusponi, J. Dreiser, J. Heidler, M. Schmidt, R. Wetter, M. Calvi, T. Schmidt, H. Pruchova, J. Krempasky, C. Quitmann, H. Brune, F. Nolting, *J. Synchrotron Radiat.* **2012**, *19*, 661.

[11] A. Barla, J. Nicolás, D. Cocco, S. M. Valvidares, J. Herrero-Martín, P. Gargiani, J. Moldes, C. Ruget, E. Pellegrin, S. Ferrer, *J. Synchrotron Radiat.* **2016**, *23*, 1507.

[12] J. Dreiser, R. Westerström, C. Piamonteze, F. Nolting, S. Rusponi, H. Brune, S. Yang, A. Popov, L. Dunsch, T. Greber, *Appl. Phys. Lett.* **2014**, *105*, 032411.

[13] a) M. Mannini, F. Pineider, C. Danieli, F. Totti, L. Sorace, P. Sainctavit, M. A. Arrio, E. Otero, L. Joly, J. C. Cezar, A. Cornia, R. Sessoli, *Nature* **2010**, *468*, 417; b) M. Mannini, F. Pineider, P. Sainctavit, C. Danieli, E. Otero, C. Sciancalepore, A. M. Talarico, M.-A. Arrio, A. Cornia, D. Gatteschi, R. Sessoli, *Nat. Mater.* **2009**, *8*, 194.

[14] F. Donati, S. Rusponi, S. Stepanow, C. Wäckerlin, A. Singha, L. Persichetti, R. Baltic, K. Diller, F. Patthey, E. Fernandes, J. Dreiser, Ž. Šljivančanin, K. Kummer, C. Nistor, P. Gambardella, H. Brune, *Science* **2016**, *352*, 318.

[15] F. D. Natterer, F. Donati, F. Patthey, H. Brune, *Phys. Rev. Lett.* **2018**, *121*, 027201.

[16] a) S. Roche, J. Åkerman, B. Beschoten, J.-C. Charlier, M. Chshiev, S. P. Dash, B. Dlubak, J. Fabian, A. Fert, M. Guimarães, F. Guinea, I. Grigorieva, C. Schönenberger, P. Seneor, C. Stampfer, S. O. Valenzuela, X. Waintal, B. van Wees, *2D Mater.* **2015**, *2*, 030202; b) A. C. Ferrari, F. Bonaccorso, V. Fal'ko, K. S. Novoselov, S. Roche, P. Bøggild, S. Borini, F. H. L. Koppens, V. Palermo, N. Pugno, J. A. Garrido, R. Sordan, A. Bianco, L. Ballerini, M. Prato, E. Lidorikis, J. Kivioja, C. Marinelli, T. Ryhänen, A. Morpurgo, J. N. Coleman, V. Nicolosi, L. Colombo, A. Fert, M. Garcia-Hernandez, A. Bachtold, G. F. Schneider, F. Guinea, C. Dekker, M. Barbone, Z. Sun, C. Galiotis, A. N. Grigorenko, G. Konstantatos, A. Kis, M. Katsnelson, L. Vandersypen, A. Loiseau, V. Morandi, D. Neumaier, E. Treossi, V. Pellegrini, M. Polini, A. Tredicucci, G. M. Williams, B. H. Hong, J.-H. Ahn, J. M. Kim, H. Zirath, B. J. van Wees, H. van der Zant, L. Occhipinti, A. Di Matteo, I. A. Kinloch, T. Seyller, E. Quesnel, X. Feng, K. Teo, N. Rupesinghe, P. Hakonen, S. R. T. Neil, Q. Tannock, T. Löfwander, J. Kinaret, *Nanoscale* **2015**, *7*, 4598.

[17] R. B. Zaripov, Y. E. Kandrashkin, K. M. Salikhov, B. Büchner, F. Liu, M. Rosenkranz, A. A. Popov, V. Kataev, *Nanoscale* **2020**, *12*, 20513.

[18] a) M. Chen, R. Guan, S. Yang, *Adv. Sci.* **2019**, *6*, 1800941; b) K. Jayanand, S. Chugh, N. Adhikari, M. Min, L. Echegoyen, A. B. Kaul, *J. Mater. Chem. C* **2020**, *8*, 3970; c) T. Wei, F. Hauke, A. Hirsch, *Acc. Chem. Res.* **2019**, *52*, 2037.

[19] J. A. Mann, J. Rodríguez-López, H. D. Abruña, W. R. Dichtel, *J. Am. Chem. Soc.* **2011**, *133*, 17614.

2105516 (7 of 7)